The Astrophysical Journal, 794:166 (9pp), 2014 October 20 doi:10.1088/0004-637X/794/2/166

IMPLICATIONS OF *VOYAGER 1* OBSERVATIONS BEYOND THE HELIOPAUSE FOR THE LOCAL INTERSTELLAR ELECTRON SPECTRUM

D. Bisschoff and M. S. Potgieter
Centre for Space Research, North-West University, 2520 Potchefstroom, South Africa; 20056950@nwu.ac.za
Received 2014 June 6; accepted 2014 August 4; published 2014 October 7

ABSTRACT

Cosmic-ray observations made by the *Voyager 1* spacecraft outside the dominant modulating influence of the heliosphere finally allow the comparison of computed galactic spectra with experimental data at lower energies. These computed spectra, based on galactic propagation models, can now be compared with observations at low energies by *Voyager 1* and at high energies by the PAMELA space detector at Earth. This improves understanding of basic propagation effects and also provides solar modulation studies with reliable input spectra from 1 MeV to 100 GeV. We set out to reproduce the *Voyager 1* electron observations in the energy range of 6–60 MeV, as well as the PAMELA electron spectrum above 10 GeV, using the GALPROP code. By varying the source spectrum and galactic diffusion parameters, specifically the rigidity dependence of spatial diffusion, we find local interstellar spectra that agree with both power-law spectra observed by *Voyager 1* beyond the heliopause. The local interstellar spectrum between ∼1 MeV and 100 GeV indicates that it is the combination of two power laws, with $E^{-(1.45\pm0.15)}$ below ∼100 MeV and $E^{-(3.15\pm0.05)}$ above ∼100 MeV. A gradual turn in the spectral shape matching the power laws is found, between 2.0 ± 0.5) GeV and (100 ± 10) MeV. According to our simplified modeling, this transition is caused primarily by galactic propagation effects. We find that the intensity beyond the heliopause at 10 MeV is (350 ± 50) electrons m^{-2} s^{-1} sr^{-1} MeV^{-1}, decreasing to (50 ± 5) electrons m^{-2} s^{-1} sr^{-1} MeV^{-1} at 100 MeV.

Key word: cosmic rays

Online-only material: color figures

1. INTRODUCTION

Voyager 1 crossed the heliopause (HP) at a distance of 121.7 AU at nearly the end of 2012 August, and then began to measure cosmic rays outside the dominant influence of the heliosphere for the first time (Stone et al. 2013; Webber & McDonald 2013). These measurements for galactic protons, helium, carbon, and oxygen and specifically for electrons, allow the comparison of computed galactic spectra with experimental data down to very low energies (a few MeV). With the addition of high-energy observations made in low earth orbit by PAMELA (Adriani et al. 2011; Menn et al. 2013), estimations of the local interstellar spectra (LISs) over a very wide range of energies can be made more reliably than done previously when making use of a comprehensive galactic propagation model, such as the GALPROP code (Strong & Moskalenko 1998; Ptuskin et al. 2006; Strong et al. 2007). We set out to achieve this goal for galactic electrons, by first computing various LISs with the GALPROP code, and then eliminating the ones that do not reproduce the reported *Voyager 1* spectra. This improves our understanding of basic galactic propagation effects, as well as serving the purpose of establishing a reliable input spectrum for galactic electrons in the energy range of 1 MeV to 100 GeV for solar modulation studies. (For a review on the importance of the LIS for solar modulation studies, see Potgieter 2013.)

It is a rather fortuitous coincidence that 100 yr after the discovery of cosmic rays at Earth, *Voyager 1* started to observe the LIS for the first time. An ongoing debate is whether *Voyager 1* has been observing the pristine LIS since 2012, or if some modulation effects could still occur between the HP and the bow shock or wherever the heliosphere commences to disturb the local interstellar medium; see, e.g., Strauss et al. (2013). If this is the case, then the observed electron spectra beyond 122 AU should rather be called HP spectra or very LISs. In this work we simply assume that the *Voyager 1* electron observations beyond 122 AU can be considered a LIS.

Stone et al. (2013) presented two possible LIS for electrons between 6 and 60 MeV based on their analysis of *Voyager 1* observations beyond the HP. They calculated two different power laws: a spectrum derived by using response functions from a pre-launch accelerator calibration and a second spectrum based on GEANT4 simulations. The uncertainty in the power index is therefore mainly determined by the systematic uncertainties in the way the *Voyager 1* electron spectra were calculated. Previous LIS estimations using radio observations at the lowest energies, such as reported by Langner et al. (2001), did not find or even consider the spectrum to be a power law in the mentioned energy range; see also Webber & Higbie (2008) and Strong et al. (2011). It was not until recently that a power-law spectrum was considered feasible at these low energies, e.g., by Potgieter & Nndanganeni (2013a), who based their modulation modeling and subsequent conclusion upon the *Voyager 1* observations when the spacecraft had moved beyond the solar wind termination shock toward the HP. They predicted a power-law shape between 1 and 100 MeV, with an index of −1.5 based on observations made in 2010 and the theoretically supported assumption that the heliospheric diffusion coefficients for electrons are almost independent of kinetic energy E below about 0.4 GeV. Reproducing PAMELA observations for 2009 above a kinetic energy where solar modulation is considered negligible, requires a completely different power law. Potgieter & Nndanganeni (2013a) reported an LIS with $E^{-(3.15\pm0.05)}$ above ∼5 GeV, with a clear spectral break occurring between ∼800 MeV and ∼2 GeV, but below this break, the LIS has a power-law form with $E^{-(1.50\pm0.15)}$. This spectral break is consistent with the computed electron spectra of Strong et al. (2011), who studied different GALPROP based models for the electron LIS, utilizing synchrotron radiation observations to constrain the low-energy

interstellar electron spectrum. Updates on the predicted LIS from solar modulation studies were made by Potgieter et al. (2013).

The two spectra reported by Stone et al. (2013) exhibit power-law indices of −1.55 based on a pre-launch calibration and a flatter −1.35 from their GEANT4 simulation, respectively. Their electron fluxes have almost the same value at the lowest reported energy (∼6–8 MeV) but progressively differs with increasing energy because of the two different power indices. We consider the two spectra as lower and upper limits for what a LIS possibly may be beyond the HP and they are separately reproduced in this study. In doing so, only two aspects are re-examined using GALPROP: the electron source spectrum and the galactic diffusion coefficient. Such a procedure was described by, e.g., Strong et al. (2011) who comprehensively tested variations to the source spectrum index using GALPROP in order to reproduce electron observations at higher energies and synchrotron emissivity estimates at lower energies. We replace the latter with *Voyager 1* measurements, but otherwise follow a plain diffusion approach, making changes to the source spectrum index and the galactic diffusion coefficient, in particular its rigidity dependence. Recently, Webber & Higbie (2013) reported a similar study, but based on their Monte Carlo diffusion model for electron propagation in the Galaxy.

The purpose of this modeling study is to establish if the LIS for electrons observed by *Voyager 1* beyond the HP could be reproduced with a plain diffusion GALPROP model at these low energies. This is done without incorporating any new physics or new assumptions. At the same time we also reproduce the electron spectrum at high energies as observed by PAMELA to investigate in the process where the spectral break occurs in the LIS, which is relevant to solar modulation studies, and if it is close to what Potgieter & Nndanganeni (2013a) found based on their solar modulation modeling. We do not attempt to find perfect fits to the two *Voyager* data sets using this modeling approach, but rather focus on the main features of these observations.

2. THE NUMERICAL MODEL AND ASSUMPTIONS

The cosmic-ray propagation equation generally has the form

$$\frac{\partial \psi}{\partial t} = S(\mathbf{r}, p) + \nabla \cdot (K \nabla \psi - \mathbf{V}\psi) + \frac{\partial}{\partial p}\left[p^2 K_p \frac{\partial}{\partial p}\frac{1}{p^2}\psi + \frac{p}{3}(\nabla \cdot \mathbf{V})\psi - \dot{p}\psi \right] - \frac{1}{\tau_f}\psi - \frac{1}{\tau_r}\psi, \quad (1)$$

where $\psi = \psi(\mathbf{r}, p, t)$ is the density per unit of total particle momentum, $S(\mathbf{r}, p)$ is the source term, K is the spatial diffusion coefficient, K_p is the momentum diffusion coefficient related to K so that $K_p K \propto p^2$, $\mathbf{V}$ is the convection velocity, $\dot{p}$ is the momentum loss rate, τ_f is the timescale for fragmentation and depends on the total spallation cross-section, and τ_r the timescale for radioactive decay. (For details on the basic theory and concepts of cosmic-ray propagation, see the review by Strong et al. 2007, see also Strong et al. 2010.)

For cosmic-ray propagation studies, the Galaxy is usually described as a cylindrical disk with a radius of ∼20 kpc and a height of up to ∼4 kpc, including the galactic halo, in which cosmic rays have a finite chance to return to the galactic disk. Assuming symmetry in azimuth leads to two spatial dimensional (2D) models that depend simply on galactocentric radius and height, whereas neglecting time dependence leads to steady-state models. These assumptions make the modeling significantly simpler so that comparisons can be made to the approach of Webber & Higbie (2013). As mentioned, we decided on using a plain diffusion approach. When implemented in the GALPROP code, it gives a 2D model with radius r, the halo height z above the galactic plane and symmetry in the angular dimension in galactocentric-cylindrical coordinates. The halo height was fixed to $z = 4$ kpc and was kept constant because varying its size can simply be counteracted by directly varying the diffusion coefficient. In this plain diffusion model, the velocity and gradient in the galactic wind is set to zero. Other parameters in the model, such as source abundance values, interstellar properties, cross-sections and gas densities were adapted straightforwardly from Ptuskin et al. (2006) and are not repeated here.

In this simplified approach, the spatial diffusion coefficient is assumed to be independent of r and z. For the case where reacceleration is not considered, it is taken as being proportional to a power law in rigidity (P) so that

$$K = \beta K_0 (P/P_{\delta 0})^{\delta}, \quad (2)$$

where $\delta = \delta_1$ for rigidity $P < P_{\delta 0}$ (the reference rigidity), $\delta = \delta_2$ for $P > P_{\delta 0}$ and with $\beta = v/c$ which is the speed of particles v, at a given rigidity relative to the speed of light, c. Here, K_0 is the scaling factor for diffusion in units of 10^{28} cm^2 s^{-1}.

The injection spectrum for electrons, as input to the source term, is assumed to be a power law in rigidity so that

$$S(P) \propto (P/P_{\alpha 0})^{\alpha} \quad (3)$$

for the injected particle density and usually contains a break in the power law with indices α_1 and α_2 below and above the reference rigidity $P_{\alpha 0}$, respectively; see also Strong & Moskalenko (1998).

In what follows, we show several electron LISs computed with the GALPROP code which solves the given transport equation using a Crank–Nicholson implicit second-order scheme. These computational runs were done via the GALPROP WebRun service[1] (Vladimirov et al. 2011). A description of the GALPROP model, and the theory it is based on, can be found in the overview by Strong et al. (2007) and references therein; see also the GALPROP Explanatory Supplement available from the GALPROP Website.

3. RESULTS: REPRODUCING THE *VOYAGER 1* ELECTRON OBSERVATIONS BEYOND THE HP

3.1. Adjusting the Electron Source Spectrum

The first objective was to establish the effects on the predicted (computed) LIS of varying only the source spectral index α in the assumed model while keeping all the other relevant parameters unchanged. This is done in comparison with the *Voyager 1* electron observations made since 2012 August beyond the HP and PAMELA electron observations at Earth during 2009. Similarly to the electron modeling done by Strong et al. (2011), α_1 was varied between −1.9 and −2.2 below a reference rigidity $P_{\alpha 0} = 4.0$ GV, whereas above this value, we kept $\alpha_2 = -2.4$ which reproduces the PAMELA spectrum satisfactorily. The

[1] http://galprop.stanford.edu/webrun/

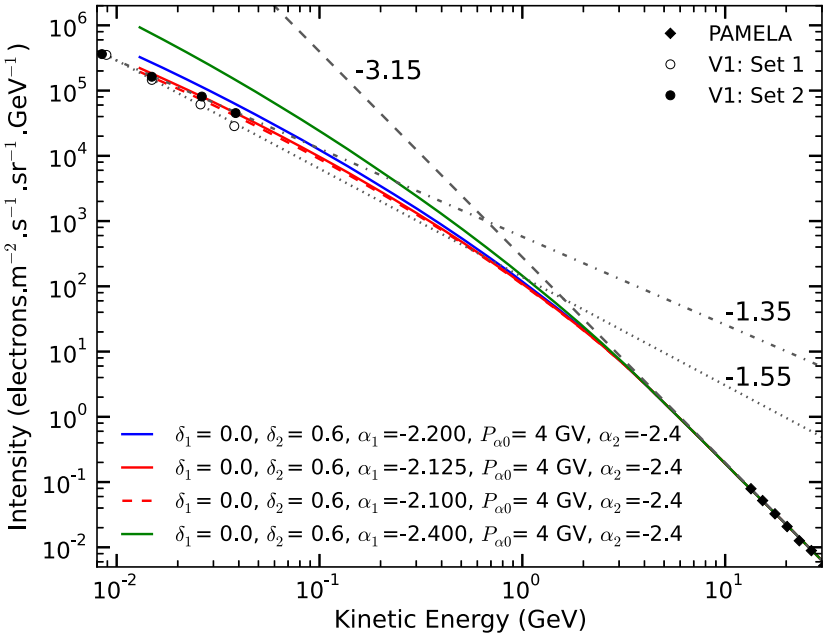

Figure 1. Electron local interstellar spectra (LISs) computed using only changes to the source spectrum index, with the purpose of reproducing both PAMELA and *Voyager 1* electron data at high and low energies, respectively. Two sets of spectra from *Voyager 1* (*V1*) were reported by Stone et al. (2013); set 1 with a power-law index of −1.55, based on a pre-launch calibration (empty circles), and set 2 with an index of −1.35 from their GEANT4 simulation (filled circles), respectively. Different values of α_1 and α_2 in Equation (3) were investigated while $\delta_1 = 0$ and $\delta_2 = 0.6$ were kept unchanged. A reference solution is shown as the green solid line with parameters as indicated. For our modeling, α_2 was kept at −2.4 to reproduce the PAMELA observations (diamonds, Adriani et al. 2011) at energies above 10 GeV but changed, as indicated, below this energy to reproduce the *V1* observations. Three computed LISs with α_1 set to −2.10 (red dashed line), −2.125 (red, solid line), and −2.20 (blue solid line) are shown. Data points from both *V1* and PAMELA are shown together with straight lines, for illustrative purposes, with power-law indices of −3.15, matching the PAMELA data (black dashed line), and −1.55 (black dotted line) and −1.35 (black dot-dash line) matching the two *V1* data sets.

(A color version of this figure is available in the online journal.)

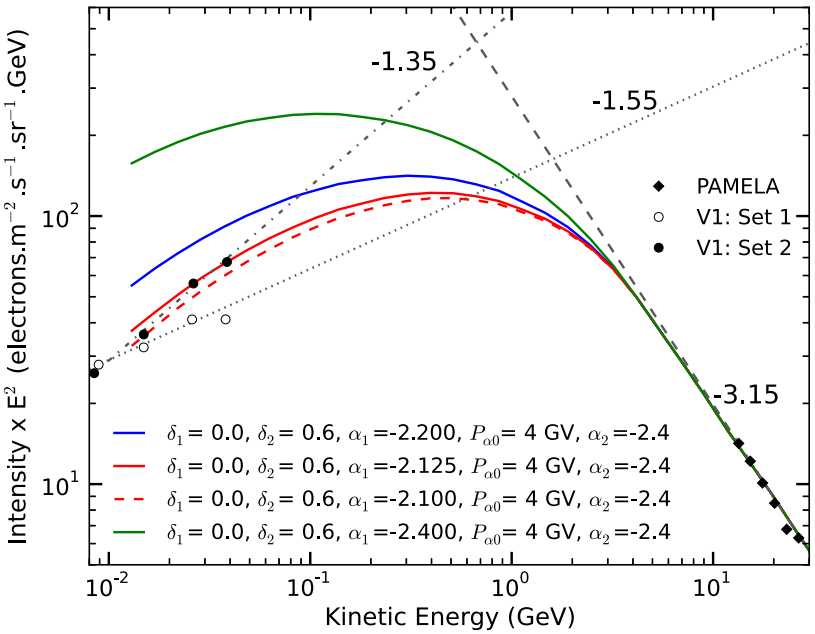

Figure 2. Same as Figure 1 but with the intensity multiplied with $E^{2.0}$. Two new LISs are computed that reproduce the observed −1.35 spectrum as suggested by the *Voyager 1* data using α_1 between −2.100 (red dashed line) and −2.125 (red solid line). Adjusting only α_1 and α_2 could not reproduce the steeper −1.55 spectrum as reported by Stone et al. (2013).

(A color version of this figure is available in the online journal.)

computed spectra are shown in Figures 1 and 2 in comparison with data from both *Voyager 1* (Stone et al. 2013) and PAMELA (Adriani et al. 2011; Menn et al. 2013). For these spectra, $\delta_1 = 0.0$, $\delta_2 = 0.6$, and $P_{\delta 0} = 3.0$ GV were kept unchanged. The PAMELA spectrum is reproduced satisfactorily above 10 GeV where solar modulation becomes progressively less. We find that values of α_1 between −2.100 and −2.125 reproduce only the observed −1.35 power-law spectrum from *Voyager 1* whereas

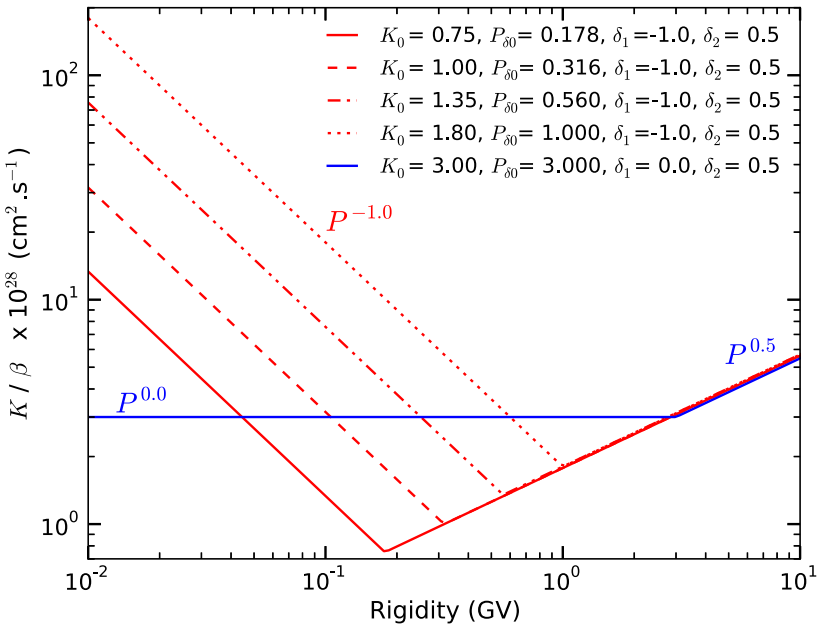

Figure 3. Rigidity dependent of the diffusion coefficient (Equation (2)) resulting from changing K_0, $P_{\delta 0}$, δ_1, and δ_2, following the example of Webber & Higbie (2013) with the purpose of reproducing the *Voyager 1* measurements at low energies as shown in Figures 1 and 2. Values resulting from $\delta_1 = -1.0$ for P below the respective breaks at $P_{\delta 0} = 0.178$, 0.316, 0.560, and 1.000 GV are shown as different red lines. For comparison values with $\delta_1 = 0.0$ below the break at 3.0 GV is shown in blue. Above 3.0 GV the rigidity dependence is the same for all assumptions, that is with $\delta_2 = 0.5$.

(A color version of this figure is available in the online journal.)

for the -1.55 observed power-law spectrum, changes in the electron source spectrum alone is insufficient to reproduce such a steep spectrum in the required low-energy range. For further comparison, a reference solution (green line) is also computed, with $\alpha_1 = \alpha_2 = -2.4$ as indicated on the figure. This solution is evidently far higher than the *Voyager 1* data but reproduces the PAMELA data as expected. The next step is to investigate the effects of changing the diffusion coefficient.

3.2. Changing the Diffusion Coefficient

In Figure 3 the diffusion coefficient as given by Equation (2), based on different assumption for K_0, $P_{\delta 0}$, δ_1, and δ_2 are shown as a function of rigidity. We here follow the example of Webber & Higbie (2013), with the purpose of reproducing the *Voyager 1* observations at low energies as were shown in Figures 1 and 2. In such an approach, the value of the diffusion coefficient is determined by K_0 when $P_{\delta 0}$ is changed for given values of δ_1 and δ_2 as indicated in the figure. For four of the five approaches, $\delta_1 = -1.0$ with δ_2 set to a value of 0.5. Here, only the break rigidity is shifted to lower values for each subsequent model to keep the corresponding K's above the break identical at the higher rigidities. The blue line represents what we consider a reference set with K independent of rigidity below 3.0 GV, that is $\delta_1 = 0.0$ but with $\delta_2 = 0.5$ above this rigidity so that the rigidity dependence is then the same for all assumptions.

The diffusion coefficients shown in Figure 3 are implemented in the GALPROP code and the resulting spectra are shown in Figure 4. The reference solution, based on the blue line in Figure 3 is also shown here in blue. For the LISs obtained with $\delta_1 = -1.0$ (varying red lines), the intensity decreases with increasing K as expected at a given low kinetic energy. The spectra (red lines) of Figure 4 all have maxima where the corresponding breaks in the rigidity dependence of K occur while they coincide above the corresponding and respective $P_{\delta 0}$. They also coincide with the reference solution above 3.0 GV (blue line). Importantly, all these LISs exhibit power laws similar to the -1.35 index indicated by the *Voyager 1* data at these lower energies. The computed LIS that is the closest to the *Voyager 1* spectrum with this power-law index, is the scenario with $K_0 = 1.35$, $P_{\delta 0} = 0.56$, and $\delta_1 = -1.0$. However, they do not reproduce the observed spectrum with the -1.55 index. For these results, the source spectrum indices are $\alpha_1 = -2.2$ and $\alpha_2 = -2.4$. To guide the eye, two straight lines are drawn through the two observed cases as shown. These LISs differ quantitatively from those produced by the Monte Carlo diffusion model of Webber & Higbie (2013), but qualitatively show the power-law trends at lower energies as required by the *Voyager 1* observations. They found a reasonable fit to the observed -1.35 spectrum using $\alpha_1 = -2.2$, $P_{\delta 0} = 1.76$ with $\delta_1 = -0.5$ and $\delta_2 = 0.5$ in their model (W. R. Webber 2014, private communication).

3.3. Improving the Rigidity Dependence of the Diffusion Coefficient

Extending this approach, we set out to search for the diffusion coefficients that will reproduce both the mentioned observed spectra while keeping the source spectrum indices, $\alpha_1 = -2.2$ and $\alpha_2 = -2.4$ unchanged. This is done by varying δ_1 instead of keeping it fixed at -1.0, as well as adjusting the break in the rigidity dependence of K through $P_{\delta 0}$ and subsequently changing also K_0. Changing δ_1 between -0.1 and -1.0, while adjusting K_0 and $P_{\delta 0}$ accordingly to keep the diffusion coefficient the same at the highest energies, the computed LISs were adjusted to eventually reproducing both the observed spectra. The best corresponding set of diffusion coefficients as a function of rigidity is shown in Figure 5, with the changes in the relevant parameters as indicted in this figure. Also shown is a diffusion coefficient that is independent of rigidity below 3.0 GV again for illustrative purposes.

Figure 6 shows the corresponding computed LISs, multiplied by $E^{2.0}$, that are based on the diffusion coefficients as shown in Figure 5. The two LISs, based on assuming $\alpha_1 = -2.2$,

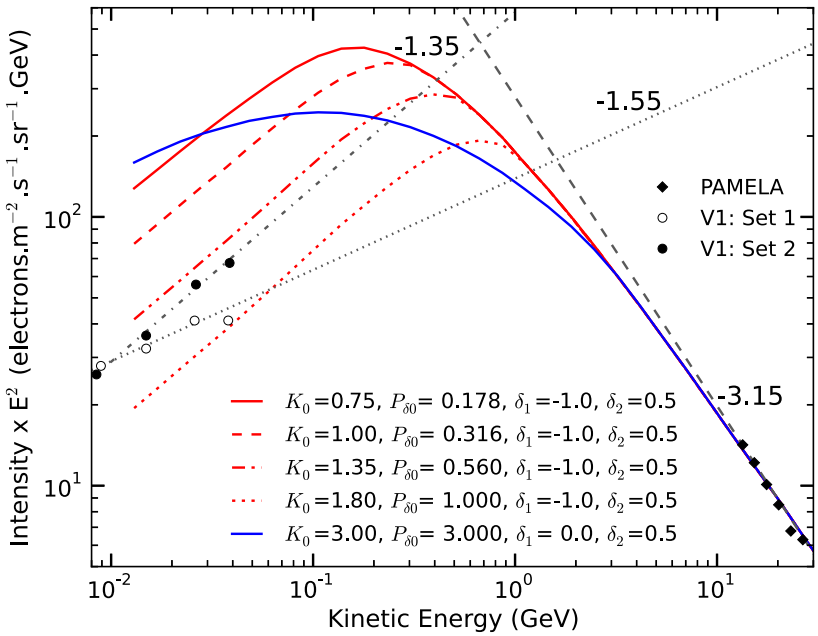

Figure 4. Resulting electron LISs, multiplied with $E^{2.0}$, computed for the various rigidity dependences of K as shown in Figure 3. As before, they are compared to the two *Voyager 1* data sets. For the LISs obtained with $\delta_1 = -1.0$ (four red lines), the intensity decreases as expected with K increasing, for a given low kinetic energy. They all exhibit power-law spectra at these lower energies similar to the observed -1.35 spectrum but do not reproduce the observed -1.55 spectrum, indicated by straight lines for illustrative purposes. The reference LIS (blue line) based on the blue line in Figure 3 is also shown.

(A color version of this figure is available in the online journal.)

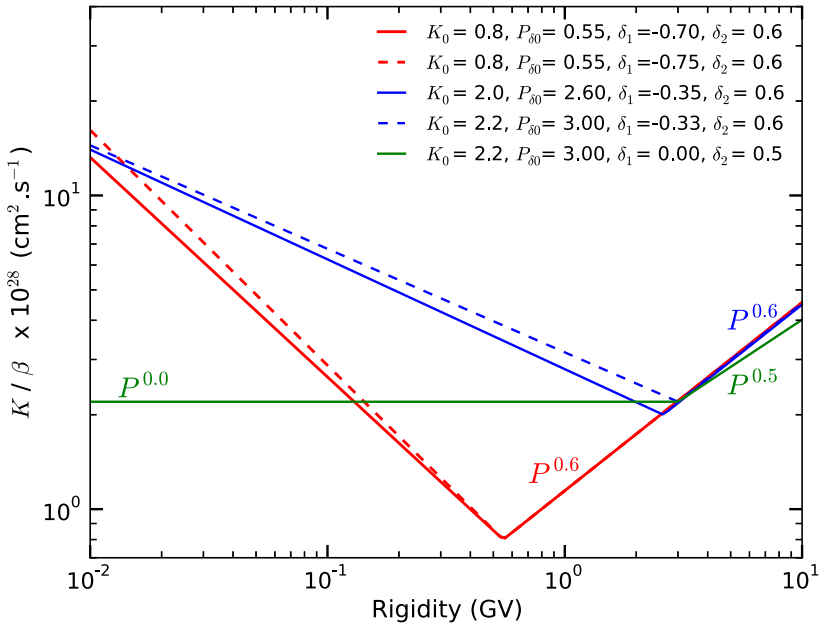

Figure 5. For the purpose of reproducing the *Voyager 1* electron measurements at low energies, the rigidity dependence of K were refined by changing δ_1, δ_2, K_0, and $P_{\delta 0}$ from those values shown in Figure 3. These changed values are indicated on the figure, and the corresponding graphs are given in blue and red, all with $\delta_2 = 0.6$. The green line serves as a reference case, with $\delta_2 = 0.5$, and relates to the blue line in Figure 3, which was also used by Ptuskin et al. (2006). Models found to reproduce the observed -1.35 spectrum are given in red and those found to reproduce the -1.55 spectrum are given in blue, as will be illustrated in the next two figures.

(A color version of this figure is available in the online journal.)

$P_{\alpha 0} = 4.0$ GV, $\alpha_2 = -2.4$, $K_0 = 0.8$, $P_{\delta 0} = 0.55$ GV, $\delta_2 = 0.6$, and δ_1 between -0.70 and -0.75 (as a margin of uncertainty in reproducing the observations), are shown as red lines, obviously reproducing the observed -1.35 spectrum rather well. These LISs have a maximum in intensity around 0.5 GeV indicating the break between the two power-law spectra as required to reproduce both the *Voyager 1* and PAMELA observations. The next two LISs, shown as blue lines, are based on varying K_0 = 2.0–2.2, $P_{\delta 0}$ = 2.6–3.0 GV, and $\delta_1 = -0.35$ to -0.33, respectively, while keeping $\alpha_1 = -2.2$, $P_{\alpha 0} = 4.0$ GV, and $\alpha_2 = -2.4$. They evidently also reproduce the observed -1.55 spectrum equally well. These LISs have a maximum around 0.9 GeV. The reference LIS (green line), with $\alpha_1 = -2.2$, $P_{\alpha 0} = 4.0$ GV, and $\alpha_2 = -2.4$, $K_0 = 2.2$, $P_{\delta 0} = 3.0$ GV, and

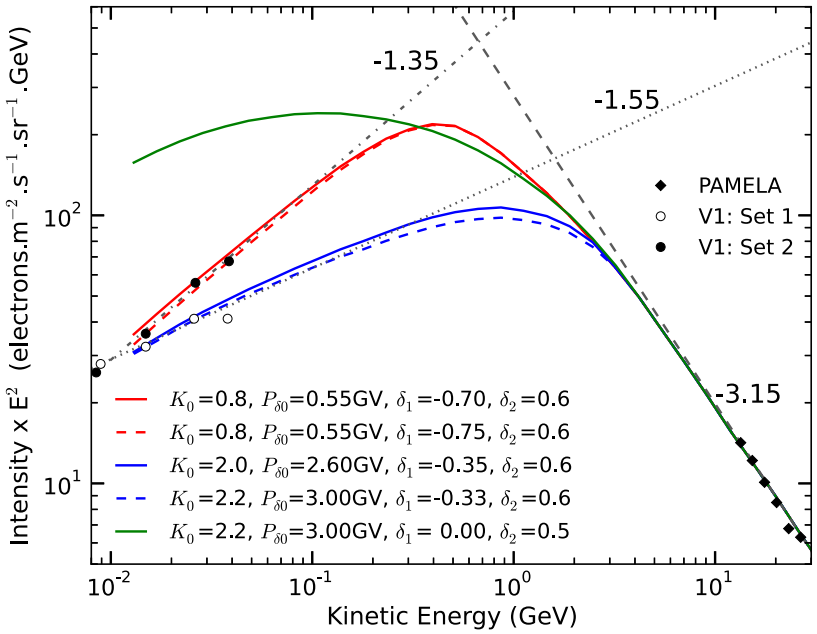

Figure 6. Computed LISs, multiplied by $E^{2.0}$, are based on the diffusion coefficients as shown in Figure 5. The two LISs based on assuming $K_0 = 0.8$, $P_{\delta 0} = 0.55$ GV and δ_1 between -0.70 and -0.75 are shown as red lines, reproducing the observed -1.35 spectrum rather well. The two LISs based on $K_0 = 2.2$, $P_{\delta 0} = 3.0$ GV, and $\delta_1 = -0.33$ are shown as blue lines, and evidently reproduce the observed -1.55 spectrum equally well. The reference LIS with $K_0 = 2.2$, $P_{\delta 0} = 3.0$ GV, and $\delta_1 = 0.0$, is shown as the green line.

(A color version of this figure is available in the online journal.)

Table 1
List of Model Parameters Used to Reproduce the Observed Electron LIS

Study Case	Power Law	α_1	$P_{\alpha 0}$ (GV)	α_2	K_0 (10^{28} cm^2 s^{-1})	δ_1	$P_{\delta 0}$ (GV)	δ_2
Green LIS	N/A	−2.4	None	−2.4	2.2	0.0	3.00	0.5
Orange LIS	−1.35	−2.1 to −2.125	4.0	−2.4	2.2	0.0	3.00	0.6
Red LIS	−1.35	−2.2	4.0	−2.4	0.8	−0.70 to −0.75	0.55	0.6
Blue LIS	−1.60	−2.2	4.0	−2.4	2.0–2.2	−0.33 to −0.35	2.6–3.0	0.6
W-H LIS	−1.35	−2.2	None	−2.2	3.0	−0.5	1.76	0.5

Notes. Model parameters used to reproduce the observed electron LIS as shown in Figures 7 and 8 and from two previous studies: W-H refers to Webber & Higbie (2013) but with updated parameters (W. R. Webber 2014, private communication) whereas green, orange, red and blue refer to the color of the LISs as shown in these two figures. K_0 is in units of 10^{28} cm^2 s^{-1} with the units of $P_{\alpha 0}$ and $P_{\delta 0}$ in GV.

$\delta_1 = 0.0$, is shown for illustrative purposes, representing the way the electron LIS was computed and taken seriously almost a decade ago. For this reference LIS the maximum is around 0.1 GeV, with the low-energy intensities significantly too high compared to the *Voyager 1* observations.

3.4. Recapping of Modeling Results

The computed LISs of our investigation are shown together in Figures 7 and 8. The relevant, corresponding parameters are summarized in Table 1. First, the computed reference LIS as shown in Figure 6 is plotted again as the green line and is based on the diffusion coefficient shown in Figure 5. The corresponding set of parameters is given in the first row of the table. Second, the two spectra shown in red in Figures 1 and 2 are now replotted as a orange band with the corresponding parameter set given in the second row of the table. (The colored band is thus bound by the two mentioned spectra, illustrating the difference between the solid red line in Figures 1 and 2 as the higher spectrum and the red dashed line as the lower spectrum.) This modeling approach reproduces only the observed -1.35 spectrum, not the -1.55 observed spectrum. Third, the computed LISs shown as two red and two blue spectra in Figure 6 are replotted here as red and blue bands, respectively. The corresponding parameter sets are given in the third and fourth row of Table 1. As before, straight lines are additionally plotted to illustrate the power laws of relevance to this study, together with the two *Voyager 1* data sets and the PAMELA observations above 10 GeV.

Inspection of the computed LISs in Figures 7 and 8 indicates that the modeling approach with δ_1 between -0.70 and -0.75, gives spectra that represent the observed -1.35 spectrum reasonably, as illustrated by the red band in Figures 7 and 8 as an indication of the margin of uncertainty caused by varying δ_1 between these two values. We consider these two LISs as the highest possible ones, obviously based on and determined by our simplified assumptions. In contrast, the LISs given as the orange band evidently reproduce the observed -1.35 spectrum less well (evidently too low around 40 MeV), indicating that this approach in obtaining an LIS seems less suitable, perhaps too simplified. Finally, the computed LISs reproducing the observed -1.55 spectrum, given as the blue band, are also reasonably

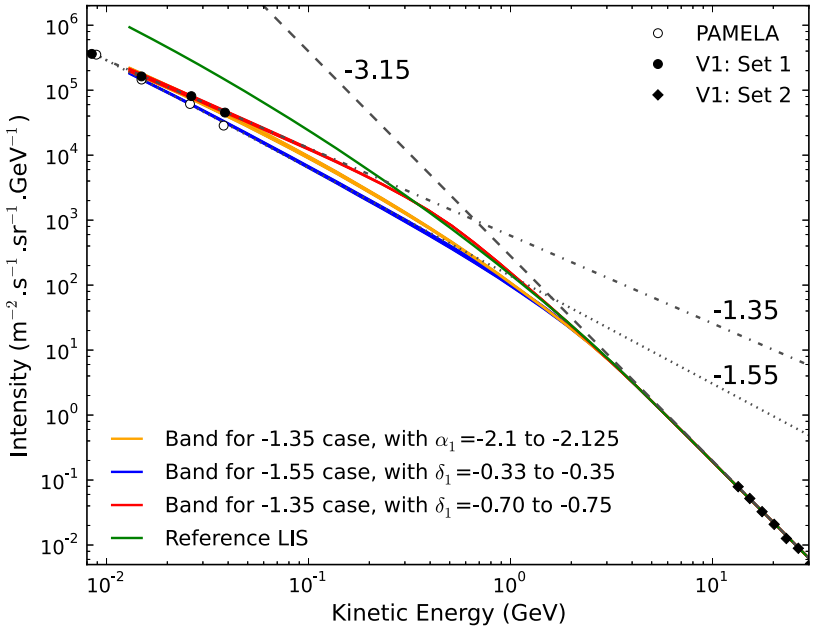

Figure 7. Resulting computed LISs found in this study that reproduce the *Voyager 1* and PAMELA (above 10 GeV) electron spectra are based on the parameters as listed in Table 1. The three sets of LISs were found through adjusting the rigidity dependence of the source spectrum and that of the diffusion coefficient when using the GALPROP code. The LIS that reproduces the observed −1.35 spectrum, is shown as the red band as a margin of uncertainty in the input parameters, and is based on the parameters shown in the third row of the table. The second LIS that reproduces also the observed −1.35 spectrum but less well than the previous case, is shown as the orange band and is based on the parameters given in the fourth row of the table. The LIS reproducing the observed −1.55 spectrum is given as a blue band, with parameters as given in the fourth row of the table. The reference LIS is shown as the green line, with parameters as given in the first row of the table. The *Voyager 1* observations (two possible sets of spectra) and PAMELA observations are shown again, together with corresponding power laws (straight lines) to guide the eye.
(A color version of this figure is available in the online journal.)

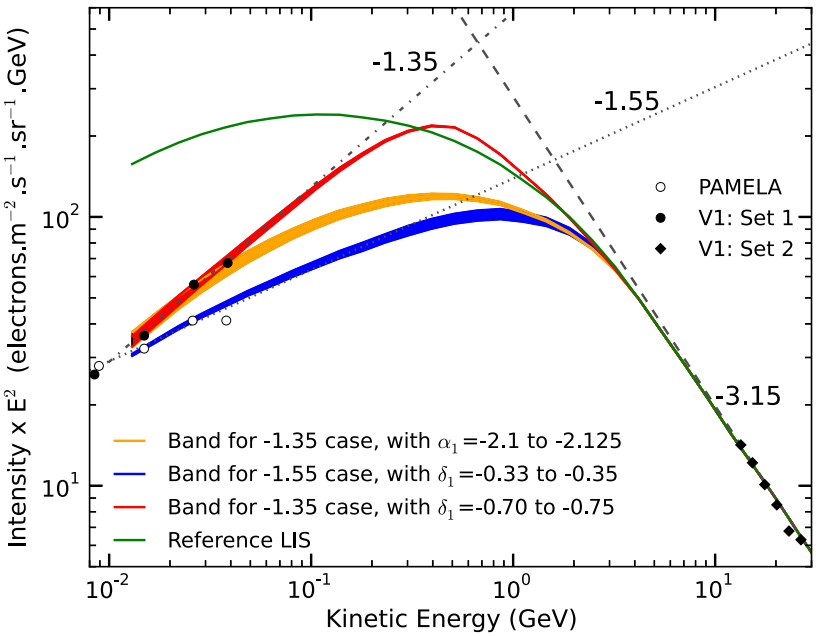

Figure 8. Same as Figure 7 but with the intensity multiplied by $E^{2.0}$ to enhance the differences.
(A color version of this figure is available in the online journal.)

good so that the approach as described above to establish this −1.55 spectrum seems justified. However, the LISs for this case are evidently not reproducing the observed power-law spectra as well as the −1.35 case (red band) because they are significantly lower than the previous ones in the mid-energy range (50–500 MeV), which is of particular importance to solar modulation studies. This aspect will be discussed further in the next section.

The parameters used by Webber & Higbie (2013) to reproduce the observed −1.35 spectrum with their model, are shown as the fifth row in the table. They seem not to require a break in the rigidity dependence of the source term whereas our results

indicate a break at 4.0 GV, where the power index changes from −2.2 (even −2.1) to −2.4. The value of K_0 is always specified at $P = P_{\delta 0}$ and because we find $P_{\delta 0} = 0.55$ (red band), it indicates that our diffusion coefficient is significantly less than theirs in the energy range from 100 MeV to 1 GeV which in our case leads to significant higher intensity at these energies. The break in the LIS is therefore quite prominent and seems consistent with the results of Potgieter & Nndanganeni (2013a) based on solar modulation studies.

4. DISCUSSION

The effects of solar modulation at energies below 30 GeV (Strauss & Potgieter 2014) in the heliosphere alter the electron LIS significantly. The total modulation between the HP and Earth (sometimes also called the modulation fraction) for 10 MeV electrons could be as large as 10^4, with a decrease of almost a factor of 400 at this energy in the heliosheath alone (region between the termination shock and HP of width between 20 and 35 AU), with a factor of two decrease just across the HP region (width of about 1 AU). It used to be difficult to calculate this number reliably because at Earth the Jovian electrons completely dominate the galactic electron flux below 30 MeV and very large uncertainties have existed in the value of the electron LIS at these very low energies. Predictions of the LIS, mainly based on GALPROP models, for 10 MeV electrons in the mid-1990's was as high as 5 × 10^3 electrons $m^{-2}\,s^{-1}\,sr^{-1}\,MeV^{-1}$. Today, owing to the *Voyager 1* observations beyond the HP, we know it can be as low as 300 electrons $m^{-2}\,s^{-1}\,sr^{-1}\,MeV^{-1}$; see, e.g., Potgieter & Nndanganeni (2013b). Very important is that we now know that the LIS has a power-law spectral shape at these low energies. This means that we can now use comprehensive solar modulation models to calculate the mentioned total modulation much more reliably and even have come to the point where we can determine a set of "standard" modulation parameters for electrons, and for other cosmic ray species. For such attempts, see Potgieter et al. (2014) and Vos et al. (2013a, 2013b).

There are also two issues about whether the two data sets from *Voyager 1* can be considered as been a pristine LIS. The first one is whether no further modulation effects could be expected beyond the HP. Strauss et al. (2013) argue that it may increase modestly (perhaps by 25%) beyond the HP for another 50 AU or so. The second issue is that what we compute here with GALPROP is an average galactic spectrum because these computations do not contain the contributions of any specific (local) sources within parsecs from the heliosphere, so that an interstellar spectrum may be different from an average galactic spectrum and even different from a very LIS or the HP spectrum that *Voyager 1* is presently observing. These issues should be seen as a work in progress.

Reproducing the *Voyager 1* data with this modeling approach results in much improved electron LISs, which, as it turned out, are much lower at energies below ∼200 MeV than previous plain diffusion model estimates and are also different from the more recent computations of Strong et al. (2011). An important aspect is that the electron LIS (below 50 GeV) clearly consists of the combination of two power laws and that the consequent break in the LIS is confirmed by our straightforward galactic propagation approach as well as by solar modulation studies. This break was also emphasized by Strong et al. (2011). Our current computations indicate that this break is at a lower energy and comes more gradual than found by Potgieter & Nndanganeni (2013a) as mentioned in the introduction. They used *Voyager 1* observations from 2010 which clearly show a power law up to 120 MeV before the break occurs. The new procedure to calculate the *Voyager 1* LISs can no longer produce intensities above ∼60 MeV (W. R. Webber 2014, private communication), which is a pity. However, Webber & Higbie (2013) also concluded that this break is gradual, starting at about 2 GeV where the spectrum is $E^{-(3.15\pm0.05)}$ and continuing down to about 100 MeV where the spectrum becomes $E^{-(1.45\pm0.15)}$. They emphasized the fact that they could reproduce the observed *Voyager* and PAMELA electron spectra with a single power-law source spectrum with index $\alpha_1 = \alpha_2 = -2.2$ whereas we get somewhat different (better) results by changing this index from $\alpha_1 = -2.2$ to $\alpha_2 = -2.4$ above $P_{\alpha 0} = 4.0$ GV.

Using source spectrum index variations only, the −1.35 power law indicated by the *Voyager 1* data was found to be easily reproduced. This requires the model to have an α_1 value of between −2.1 and −2.125, with all the other parameters unchanged (first row of Table 1). For the −1.55 power law, no fit was found by using this method of varying only the source spectrum index at lower rigidity. Implementing a similar approach as Webber & Higbie (2013), of changing the rigidity dependence of the diffusion coefficient, resulted in LISs that differ somewhat from their spectra, which may be attributed to differences between GALPROP and their Monte Carlo diffusion model. Our adjustments to this approach reproduce both the power laws as indicated by the *Voyager 1* data with $\alpha_1 = -2.2$ and δ_1 between −0.70 and −0.75 (third row of Table 1) reproducing the −1.35 power law and $\alpha_1 = -2.2$ with δ_1 between −0.33 and −0.35 (fourth row of Table 1) for the observed −1.55 power law.

The realization that a power law is also exhibited at the very low energies came when *Voyager 1* observed such a spectrum once it had gone beyond the solar wind termination shock. The solar modulation modeling and application of turbulence theory for galactic electron in the heliosphere led Potgieter & Nndanganeni (2013a, 2013b) to predict that the electron HP spectrum and subsequently the LIS must have such a spectral shape. Making this conclusion was complicated by the fact that *Voyager 1* had observed a factor of ∼400 increase for ∼10 MeV electrons from late 2004 (at ∼94 AU), when it crossed the termination shock, to 2012 August (at 121.7 AU), when it crossed the HP. While traversing the relatively narrow HP region, these electrons increased by a factor of ∼2. Although the power-law spectral shape became quite clear, the value of the differential intensity was more difficult to determine. This was made even more complicated by the two procedures used by the *Voyager* team to calculate the differential flux from counting rates. At present, it is reasonable to give the intensity beyond the HP at 10 MeV as (350 ± 50) electrons $m^{-2}\,s^{-1}\,sr^{-1}\,MeV^{-1}$ decreasing to (50 ± 5) electrons $m^{-2}\,s^{-1}\,sr^{-1}\,MeV^{-1}$ at 100 MeV, when the −1.35 spectrum is used.

5. CONCLUSIONS

The LIS for galactic electrons between about ∼1 MeV and 100 GeV indicates that it is the combination of two power laws, with $E^{-(1.45\pm0.15)}$ below ∼100 MeV but with $E^{-(3.15\pm0.05)}$ above energies where solar modulation is negligible. Our galactic propagation modeling approach can reproduce easily the observed −1.35 spectrum by modestly adjusting the power index of the source spectrum together with reasonable adjustments of the rigidity dependence of the spatial diffusion coefficient as shown in Table 1, labeled as the red LIS, also shown in red in Figures 7 and 8. It was not as easy to reproduce the observed

−1.55 spectrum with our straightforward approach. The corresponding computed LIS seems less convincing (in terms of it spectral shape), with significant lower intensity between 50 MeV and 1 GeV which will have a considerable impact, if indeed the case, on solar modulation studies where the prime objective is to determine reliably a "standard" set of modulation parameters for electrons during at least solar minimum activity conditions.

Focusing on the observed −1.35 spectrum, as a biased preference on our side, indicates that the LIS exhibits a gradual turn in the spectral shape, starting from (2.0 ± 0.5) GeV, ending at (100 ± 10) MeV. According to our simplified modeling, this break is caused primarily by galactic propagation effects, as presented in Figure 5 and summarized in Table 1. We find for this spectrum that the electron intensity beyond the HP at 10 MeV is (350 ± 50) electrons $m^{-2}\ s^{-1}\ sr^{-1}\ MeV^{-1}$, decreasing to (50 ± 5) electrons $m^{-2}\ s^{-1}\ sr^{-1}\ MeV^{-1}$ at 100 MeV.

The authors wish to thank the GALPROP developers and their funding bodies for access to and use of the GALPROP WebRun service. We also thank Bill Webber and Mirko Boezio for fruitful discussions. D.B. thanks the South African National Research Foundation (NRF) for providing him with a bursary for his PhD studies. M.S.P. acknowledges the financial support of the NRF under the Incentive and Competitive Funding for Rated Researchers, grant Nos. 87820 and 68198.

REFERENCES

Adriani, O., Barbarino, G. C., Bazilevskaya, G. A., et al. 2011, PhRvL, 106, 201101
Langner, U. W., de Jager, O. C., & Potgieter, M. S. 2001, AdSpR, 27, 517
Menn, W., Adriani, O., Barbarino, G. C., et al. 2013, AdSpR, 51, 209
Potgieter, M. S. 2013, LRSP, 10, 3
Potgieter, M. S., & Nndanganeni, R. R. 2013a, APh, 48, 25
Potgieter, M. S., & Nndanganeni, R. R. 2013b, Ap&SS, 345, 33
Potgieter, M. S., Vos, E. E., & Nndanganeni, R. R. 2014, in Proc. 14th ICATPP, Astroparticle, Particle, Space Physics, and Detectors for Physics Applications, ed. S. Giani et al. (Singapore: World Scientific), 204
Potgieter, M. S., Vos, E. E., Nndanganeni, R. R., Boezio, M., & Munini, R. 2013, ICRC 33, icrc2013-0056
Ptuskin, V. S., Moskalenko, I. V., Jones, F. C., Strong, A. W., & Zirakashvili, V. N. 2006, ApJ, 642, 902
Stone, E. C., Cummings, A. C., McDonald, F. B., et al. 2013, Sci, 341, 150
Strauss, R. D., & Potgieter, M. S. 2014, AdSpR, 53, 1015
Strauss, R. D., Potgieter, M. S., Ferreira, S. E. S., Fichtner, H., & Scherer, K. 2013, ApJL, 765, L18
Strong, A. W., & Moskalenko, I. V. 1998, ApJ, 509, 212
Strong, A. W., Moskalenko, I. V., & Ptuskin, V. S. 2007, ARNPS, 57, 285
Strong, A. W., Orlando, E., & Jaffe, T. R. 2011, A&A, 534, A54
Strong, A. W., Porter, T. A., Digel, S. W., et al. 2010, ApJL, 722, L58
Vladimirov, A. E., Digel, S. W., Jóhannesson, G., et al. 2011, CoPhC, 182, 1156
Vos, E. E., Potgieter, M. S., Boezio, M., et al. 2013a, ICRC 33, icrc2013-0273
Vos, E. E., Potgieter, M. S., Boezio, M., et al. 2013b, ICRC 33, icrc2013-0276
Webber, W. R., & Higbie, P. R. 2008, JGR, 113, 11106
Webber, W. R., & Higbie, P. R. 2013, arXiv:1308.6598
Webber, W. R., & McDonald, F. B. 2013, JGR, 40, 1665